Volume 2
Number 6
November 2023
Pages 1325–1660

Sensors & Diagnostics

rsc.li/sensors

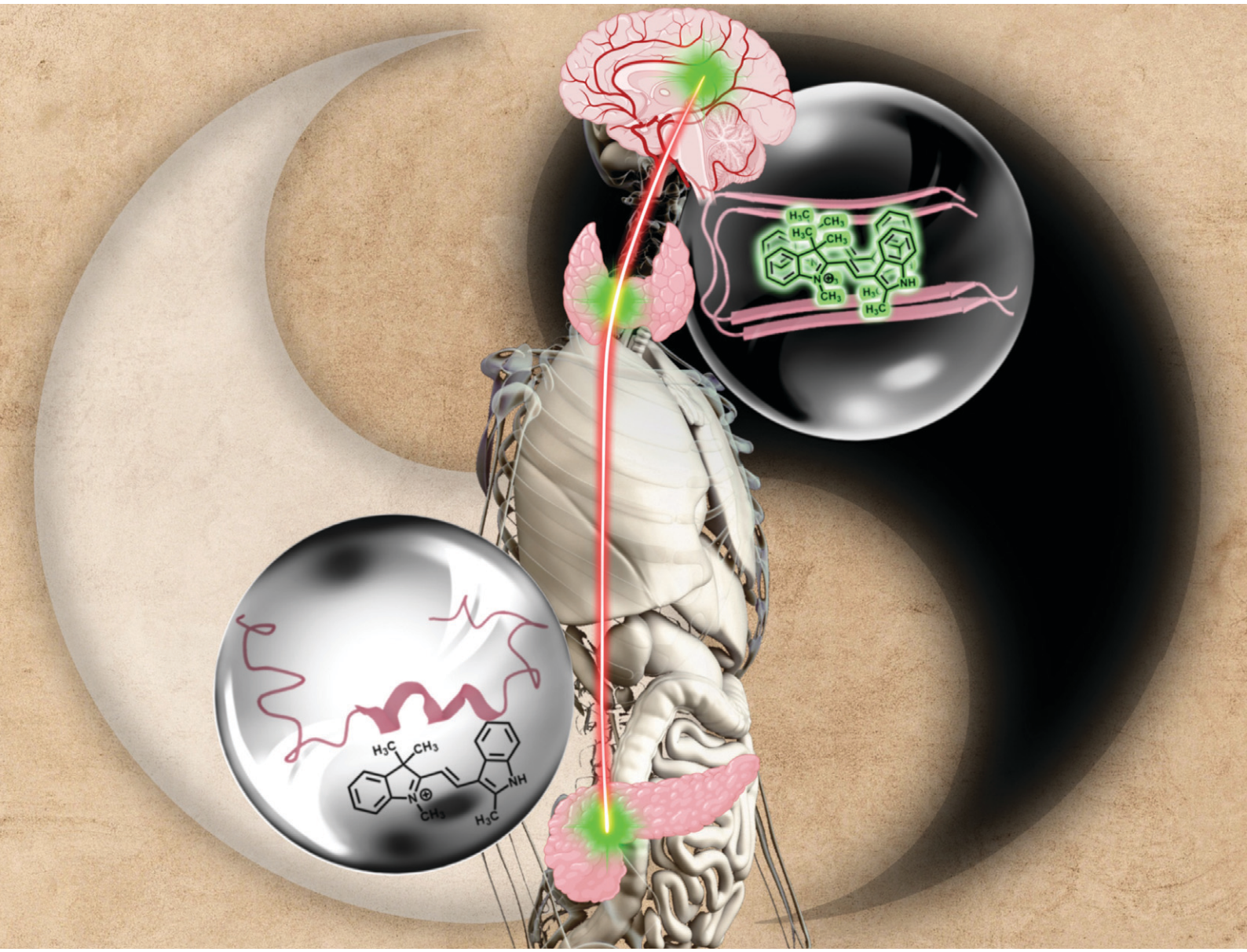

ISSN 2635-0998

ROYAL SOCIETY OF CHEMISTRY

PAPER
Jie Zheng *et al.*
Multi-target amyloid probing and inhibition using basic orange fluorescence

Sensors & Diagnostics

PAPER

View Article Online
View Journal | View Issue

Cite this: *Sens. Diagn.*, 2023, **2**, 1469

Multi-target amyloid probing and inhibition using basic orange fluorescence†

Yijing Tang,[a] Dong Zhang,[a] Xiong Gong [b] and Jie Zheng *[a]

Misfolding and aggregation of amyloid peptides are critical pathological events in numerous protein misfolding diseases (PMDs), such as Alzheimer's disease (AD), type II diabetes (T2D), and medullary thyroid carcinoma (MTC). While developing effective amyloid detectors and inhibitors to probe and prevent amyloid aggregation is a crucial diagnostic and therapeutic strategy for treating debilitating diseases, it is important to recognize that amyloid detection and amyloid prevention are two distinct strategies for developing pharmaceutical drugs. Here, we reported novel fluorescent BO21 as a versatile "dual-function, multi-target" amyloid probe and inhibitor for detecting and preventing amyloid aggregates of different sequences (Aβ, hIAPP, or hCT) and sizes (monomers, oligomers, or fibrils). As an amyloid probe, BO21 demonstrated a higher sensitivity and binding affinity to oligomeric and fibrillar amyloids compared to ThT, resulting in up to 18–39 fold fluorescence enhancements. As an amyloid inhibitor, BO21 also demonstrated its strong amyloid inhibition property by effectively preventing amyloid aggregation, disaggregating preformed amyloid fibrils, and reducing amyloid-induced cytotoxicity. The findings of this study offer a new perspective for the discovery of dual-functional amyloid probes and inhibitors, which have the potential to greatly expand the diagnostic and therapeutic treatments available for PMDs.

Received 23rd May 2023,
Accepted 18th August 2023

DOI: 10.1039/d3sd00124e

rsc.li/sensors

1. Introduction

Amyloid proteins are a unique class of biomolecules that have the ability to self-assemble into a variety of structures such as oligomers, protofibrils, and fibrils, all of which are rich in β-structures.[1,2] These structures are considered as pathological hallmarks in a number of protein-misfolding diseases (PMDs),[1,3–7] *e.g.*, amyloid-β (Aβ) in Alzheimer's disease (AD), human islet amyloid polypeptide (hIAPP) in type II diabetes (T2D), human calcitonin (hCT) in medullary thyroid carcinoma (MTC), and α-synuclein (α-syn) in Parkinson's disease (PD). These progressive PMDs typically do not exhibit apparent symptoms during their early stages, emphasizing the importance of detecting these diseases at their earliest stages before asymptomatic progression renders them irreversible.[8,9]

Fluorophores with a fluorescence turn-on mechanism, including thioflavin-T (ThT) and Congo red (CR), are widely used as probes to detect amyloid aggregates due to their simple read-out, easy instrumentation, rapid fluorescence response, and high sensitivity.[10–13] Among these fluorophores, ThT (Fig. 1b) was the first fluorescent probe used for amyloid detection and its history can be tracked back to 1959.[14] ThT is a planar-like molecular rotor that contains both an electron acceptor (benzothiazole) and donor (aniline), allowing it to freely rotate around the C–C bond in an unbound state. However, upon binding to the hydrophobic β-sheet grooves of amyloid fibrils, ThT undergoes non-radiative torsional twisting of C–C bonds, resulting in a dramatic enhancement in fluorescence emission.[15] ThT is considered as a gold-standard probe for (i) quantifying amyloid formation,[16–18] (ii) determining binding sites in amyloid structures,[19,20] (iii) detecting and differentiating amyloid aggregates with different structural features,[21,22] (iv) staining amyloid aggregates *in vitro*, *ex vivo*, and *in vivo*,[23,24] and (v) screening amyloid inhibitors for PMDs.[25,26] On the other hand, ThT has certain limitations. For example, it exhibits almost exclusive binding selectivity toward amyloid fibrils[27] and not toward amyloid oligomers that are considered to be the most toxic species. Furthermore, ThT is known to experience major interference from the autofluorescence of the biological matrix, which results in a strong background signal.[28,29] Recent studies have shown that only ~10% of the bound ThT in amyloid solution contributes to the observed fluorescence enhancement,[30] suggesting that ThT may not be an accurate measure of amyloid fibrils due to non-specific binding.

[a] *Department of Chemical, Biomolecular, and Corrosion Engineering, The University of Akron, Ohio, USA. E-mail: zhengj@uakron.edu*
[b] *School of Polymer Science and Polymer Engineering, The University of Akron, Ohio, USA*

† Electronic supplementary information (ESI) available. See DOI: https://doi.org/10.1039/d3sd00124e

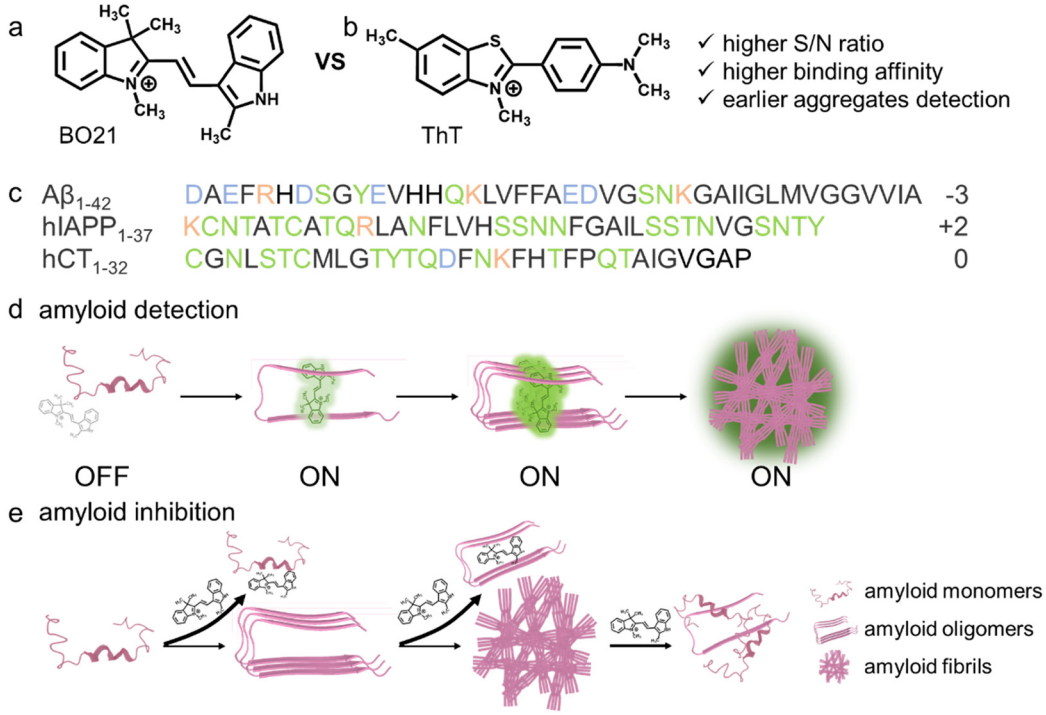

Fig. 1 Dual-functional BO21 fluorescence for amyloid detection and inhibition. Chemical structure of (a) BO21 and (b) ThT. (c) Sequence of Aβ, hIAPP, and hCT. Color ID: positively charged residues (orange letters), negatively charged residues (blue letters), polar residues (green), and non-polar residues (black). (d) BO21 serves as a general amyloid probe with an "off–on" switch to detect various amyloid aggregates. (e) BO21 functions as an amyloid inhibitor to prevent amyloid aggregation *via* different pathways.

It is crucial to search for alternative fluorescent compounds that exhibit higher binding affinity and selectivity towards amyloid oligomers, as well as larger differences in fluorescence between the free and amyloid-bound forms. Basic orange 21 (BO21) is a cationic polymethine dye,[31,32] with a structure comprising a methyl indolinium group and an indole group connected by a bridging C=C bond (Fig. 1a). As a molecular rotor, upon photoexcitation BO21 undergoes a torsional motion due to either the indolinium or indole rings rotating with respect to the H–C=C–H plane, which leads to the formation of the twisted intramolecular charge transfer (TICT) state.[33] When BO21 molecules aggregate or bind to targets, the free rotation of its molecular fragments is restricted, preventing the torsional movements.[34] This suppression of nonradiative decay modes results in an elevated quantum yield. More importantly, BO21 outperforms other fluorescent dyes due to several advantages. Firstly, BO21 has far higher fluorescence polarization (FP) than most fluorophores in water.[31] Secondly, the quantum yield of BO21 in water is much lower than that of similarly-sized fluorescein, which is a consequence of its short lifetime.[35] Lastly, BO21 has been extensively used in cellular biological studies due to its low cytotoxicity,[35–39] making it a promising candidate for biomedical applications.

Considering that both "inhibition" and "detection" of amyloid aggregates are essentially governed by molecular interactions between amyloid proteins and probe molecules, any molecule that exhibits high binding affinity with amyloids could potentially function as both an amyloid detector and inhibitor.[40,41] Toward this goal, we proposed to examine the potential functions of BO21 as both an amyloid probe and inhibitor for monitoring, detecting, and altering amyloid aggregation of three different amyloid proteins (namely, Aβ, hIAPP, and hCT, Fig. 1c). In comparison to ThT that is the most extensively studied and commonly used amyloid probe, BO21 exhibits a distinctive off–on fluorescence response when in the presence of amyloid aggregates, offering several remarkable advantages: (i) an ultrahigh signal-to-noise (S/N) ratio with integrated background minimization and accurate signal amplification, (ii) an exceptional binding affinity to amyloid aggregates, (iii) the ability to detect oligomeric intermediates formed during the early stages of fibril formation, and (iv) the capacity to differentiate between amyloid monomers, oligomers, and fibrils based on distinct fluorescence intensities (Fig. 1d). In addition to its role as an amyloid probe, BO21 also functions as an amyloid inhibitor, able to modify the amyloid aggregation pathway, fibril morphology, and secondary structure distributions through different pathways. BO21 can inhibit amyloid fibrillization by targeting small aggregates, disassemble preformed amyloid fibrils, and alleviate amyloid-associated cytotoxicity (Fig. 1e). More importantly, extensive efforts have been made in the amyloid research field to develop amyloid detectors and inhibitors. However, as illustrated in Fig. 2, most of these strategies do not possess

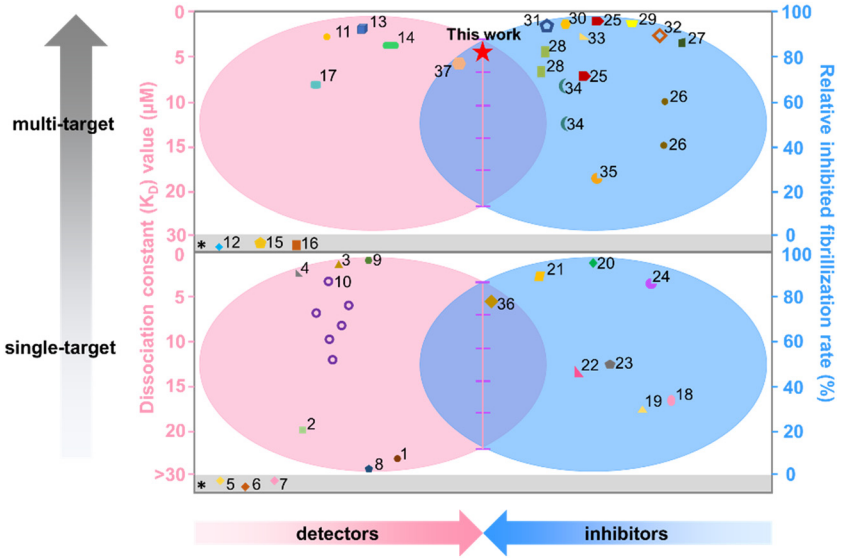

Fig. 2 Functional comparison of different amyloid detectors and inhibitors in terms of the K_D value (red) and relative inhibited fibrillization rate (blue). References* indicate that neither the K_D value nor the relative amyloid fibrillization rate is available in the cited literature. All references here are also listed in Table S1.†

the ability to combine these two functions. Conventional design approaches are primarily limited to a single function (amyloid detectors[42–46] or inhibitors[47–50]) or a single amyloid protein[51] (Aβ, hIAPP, or hCT), and have yet to yield successful drugs on the market. Our study presents, for the first time, BO21 as a "multi-target, dual-function" amyloid probe and inhibitor, offering a promising avenue for (pre)clinical strategies in the diagnosis and treatment of PMDs.

2. Results and discussion

2.1. Aggregation- and concentration-dependent fluorescence emission of BO21 independent of amyloid sequences

Firstly, we carried out a series of spectroscopic tests to study the binding-induced emission of BO21 when interacting with (i) different amyloid proteins of Aβ, hIAPP, and hCT and (ii) different aggregation species of amyloid proteins from monomers and oligomers to fibrils at different BO21 : amyloid molar ratios of 1 : 0.625–1 : 40. As shown in Fig. 3a, at first glance, BO21 exhibited a "concentration and conformational-dependent, sequence-independent" fluorescence emission property. *i.e.*, for all three types of amyloid peptides, the emission intensity of BO21 consistently increased with the gradual rise in amyloid aggregate concentration, exhibiting a preferential binding order of amyloid fibrils > amyloid oligomers > amyloid monomers. Specifically, as compared to the blank background fluorescence signal of 4.73 a.u. for 1 μM BO21 alone, when BO21 (1 μM) was co-incubated with Aβ, hIAPP, and hCT monomers (0.625–40 μM), all three BO21–amyloid systems exhibited weak emission peaks at 540 nm, as indicated by the fluorescence intensity of 5.96–50.6 a.u., 6.60–16.5 a.u., and 5.30–12.4 a.u., respectively, indicating that BO21 had a very low binding affinity to amyloid monomers. Among these three amyloid monomers, BO21–Aβ monomers exhibited a significant increase in fluorescence intensity, especially at higher concentrations of 20–40 μM Aβ monomers. This can be attributed to the higher aggregation rate of Aβ (Fig. 5a), resulting in a higher packing density of Aβ aggregates to restrict the free rotation of BO21.

Conversely, upon introducing BO21 to amyloid oligomers, the fluorescence intensities at 540 nm displayed a gradual increase from 9.93 to 94.0 a.u. for Aβ oligomers, from 6.39 to 147 a.u. for hIAPP oligomers, and from 25.9 to 107 a.u. for hCT oligomers, as the amyloid concentration increased from 0.625 to 40 μM. The fluorescence enhancement became more pronounced in the BO21–amyloid fibril systems, with the highest fluorescence intensities at 540 nm observed to be 184, 330, and 387 a.u. for 40 μM Aβ, hIAPP, and hCT fibrils, respectively. Quantitively, the binding affinities (K_D) of BO21 to different amyloid aggregates from monomers and oligomers to fibrils were determined through the simplified 1 : 1 binding model.[52,53] The fluorescence intensity increased at 540 nm with titration was used to quantify the binding affinities, which were found to be 34 nM, 15 nM, and 139 nM for Aβ monomers, oligomers, and fibrils, 46 nM, 18 nM, and 115 nM for hIAPP monomers, oligomers, and fibrils, and 29 nM, 36 nM, and 240 nM for hCT monomers, oligomers, and fibrils, respectively. These results confirm strong and general binding between BO21 and different amyloid aggregates (Table S2 and Fig. S1†). Fluorescence titration results demonstrate a binding affinity order of oligomers > monomers > fibrils across different amyloid seeds. The fluorescence emission intensity observed for different types of amyloid aggregates can be attributed to the ability of BO21 to bind to the general β sheet-rich structure of amyloid oligomers and fibrils. Such BO21–amyloid binding leads to a

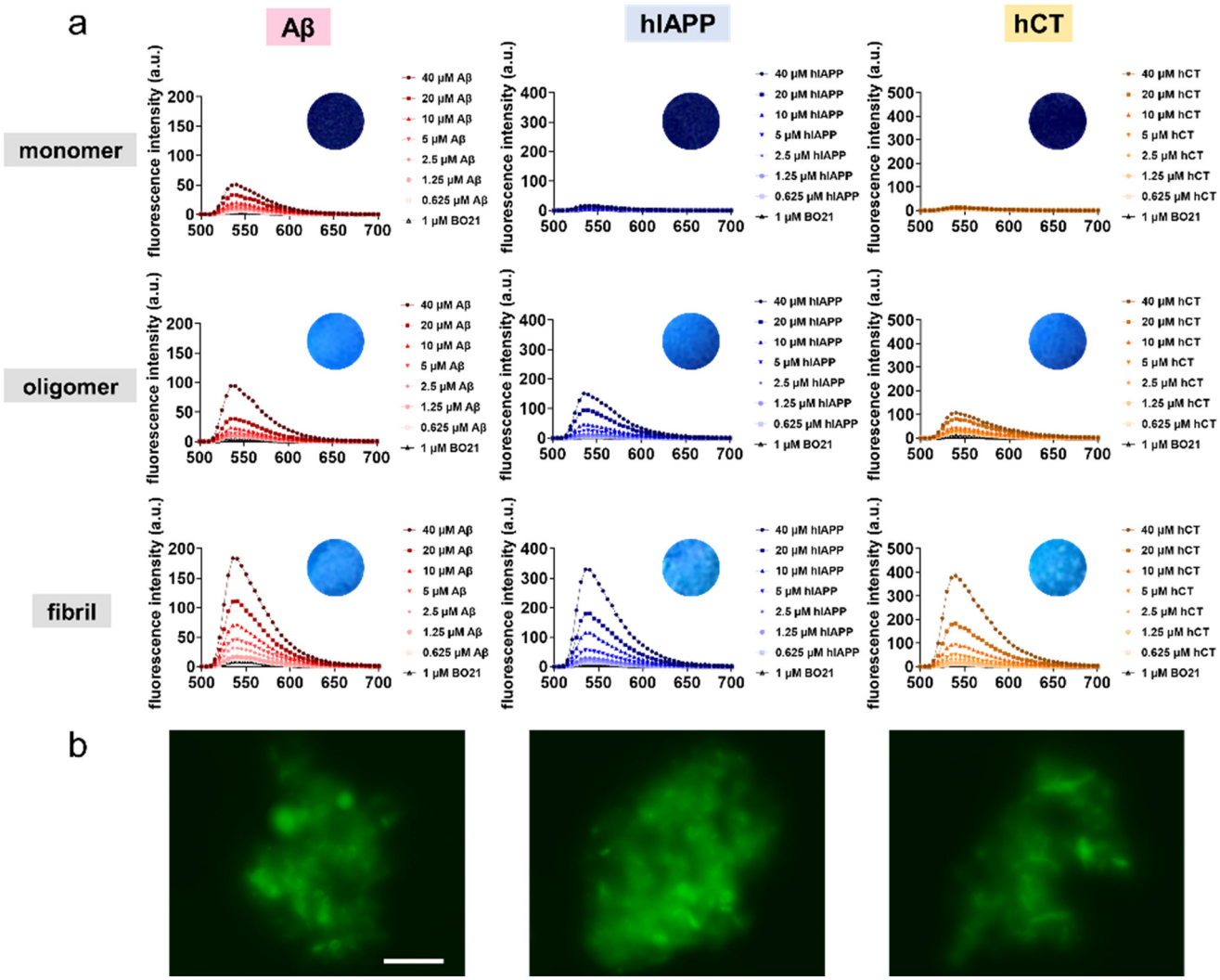

Fig. 3 BO21 exhibits an aggregation- and concentration-dependent fluorescence emissive property that is independent of amyloid sequences. (a) Fluorescence spectra and optical photos (insets) of BO21 (1 μM) in the absence (black) and presence (colored) of monomeric (1st row), oligomeric (2nd row), and fibrillar (3rd row) aggregates of Aβ (1st column), hIAPP (2nd column), and hCT (3rd column), showing the sequence-independent fluorescence emissive property of BO21 that is aggregation- and concentration-dependent. (b) Representative fluorescence images of amyloid fibrils stained by BO21. Scale bars are 45 μM. Samples were prepared in BO21 (1 μM)–PBS buffer solution (10 mM, pH = 7.4) with different concentrations of amyloid seeds (amyloid : BO21 = 0.625–40) in a 96-well plate at room temperature and recorded between 500 and 700 nm with an excitation wavelength of 470 nm.

decrease in conformational freedom and rotational restriction of the BO21 fluorophore. In other words, when BO21 binds to monomeric amyloids with random coil structures, it is able to retain its freely rotational state, as reflected in the lower fluorescence intensity observed.

Seeing is believing. Visual inspection of the binding and detection of amyloid aggregates by BO21 was achieved through fluorescence imaging. Under UV photoexcitation, mixtures of amyloid oligomers and fibrils with BO21 showed strong fluorescence, while mixtures of native amyloids and BO21 emitted almost no light (inset images in Fig. 3a). Further fluorescence imaging was performed by staining amyloid oligomers and fibrils with 1 μM BO21, as shown in Fig. 3b and S2.† The images confirmed that BO21 failed to probe amyloid monomers, as evidenced by the all-black images, while it became readily visible when co-incubated with amyloid oligomers and fibrils. Evidently, the fluorescence emission intensity of BO21 decreases in the presence of amyloid fibrils, followed by amyloid oligomers and amyloid monomers. This reduction in fluorescence emission aligns with the gradual decrease in the β-sheet structure observed from amyloid fibrils to amyloid oligomers and amyloid monomers. This finding indicates that the fluorescence emission of BO21 is attributed to its interaction with the β-sheet structure of amyloid aggregation, irrespective of the specific amyloid sequences investigated. Mechanistically, the binding of BO21 to the β-sheet structure of amyloid aggregates restricts the free rotation of BO21, leading to increased radiative recombination and fluorescence emission.

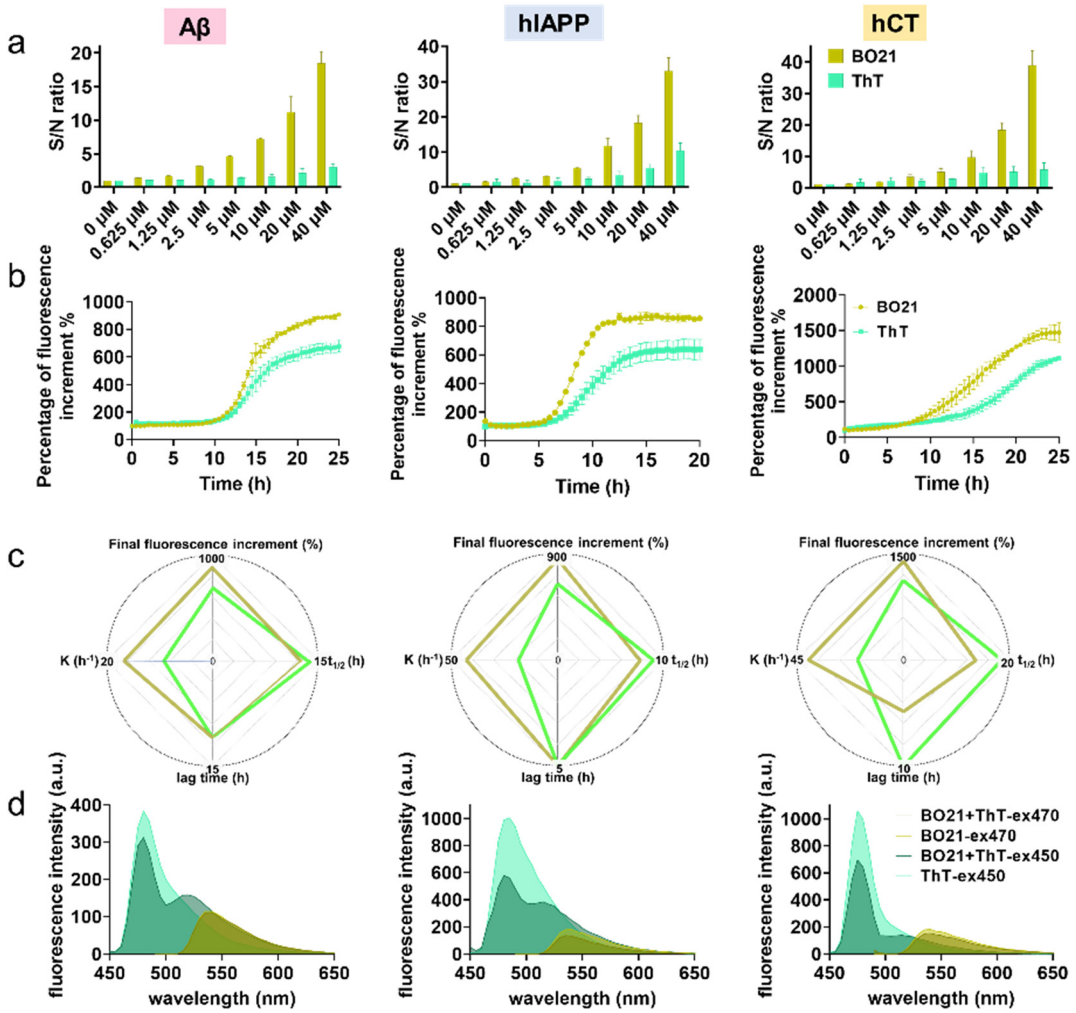

Fig. 4 Comparative monitoring and detection of amyloid fibrillation by BO21 and ThT. (a) Signal-to-noise (S/N) ratio comparison of ThT (green) and BO21 (dark yellow) probes for detecting Aβ (1st column), hIAPP (2nd column), and hCT (3rd column) aggregates at concentrations ranging from 0 to 40 μM. (b) Fluorescence profiles and (c) radar charts for evaluating the performance of ThT and BO21 probes in detecting Aβ, hIAPP, and hCT aggregates based on four criteria: final fluorescence increment, aggregation rate (k), aggregation half time ($t_{1/2}$), and lag-phase time. (d) Competitive binding of ThT and BO21 to Aβ, hIAPP, and hCT fibrils under the same excitation. Samples were prepared in BO21 (1 μM)–PBS buffer solution (10 mM, pH = 7.4)/ThT (1 μM)–PBS buffer solution (10 mM, pH = 7.4) with different concentrations of amyloid seeds (amyloid : BO21 = 0.625–40) in a 96-well plate at room temperature and recorded between 500 and 700 nm/450 and 650 nm with an excitation wavelength of 470 nm/450 nm.

2.2. Comparison of BO21 and ThT as fluorescent probes for detecting amyloid aggregates

In order to quantitatively detect amyloid using BO21 and ThT (a gold standard amyloid probe), a titration experiment was conducted by measuring fluorescence spectra in PBS at a series of amyloid mature fibril concentrations (0–40 μM) (Fig. S3†). As a control, in the absence of amyloid fibrils, ThT alone showed a fluorescence intensity of 190 a.u. due to its inherent fluorescence property in aqueous solution, thus yielding an undesirable background noise signal. In contrast, BO21 showed a significantly lower background signal of only 4.75 a.u., which was 1/40th of the ThT background signal. The low background signal of BO21 could be attributed to its high solubility in aqueous solution, which minimized its non-specific binding and fluorescence background. This characteristic of BO21 provided essential conditions for achieving an ultrahigh signal-to-noise (S/N) ratio. As shown in Fig. 4a, BO21 exhibited exceptional S/N ratios ranging from 1.37 to 18.4, 1.57 to 33.0, and 1.21 to 38.9 upon binding to 0.625 to 40 μM Aβ, hIAPP, and hCT fibrils, respectively. In comparison, ThT yielded lower S/N ratios, ranging from 1.05 to 2.98 for Aβ fibrils, 1.61 to 10.4 for hIAPP fibrils, and 1.66 to 5.73 for hCT fibrils. Additionally, BO21 demonstrated a superior linear fit with all types of amyloid fibrils compared to ThT, as evidenced by its higher R^2 values of 0.9839, 0.9930, and 0.9982 for Aβ, hIAPP, and hCT fibrils, respectively. In contrast, ThT exhibited lower R^2 values ranging from 0.7820 to 0.9968. The superior S/N ratio and linearity of BO21 can be attributed to its low background signal and increased

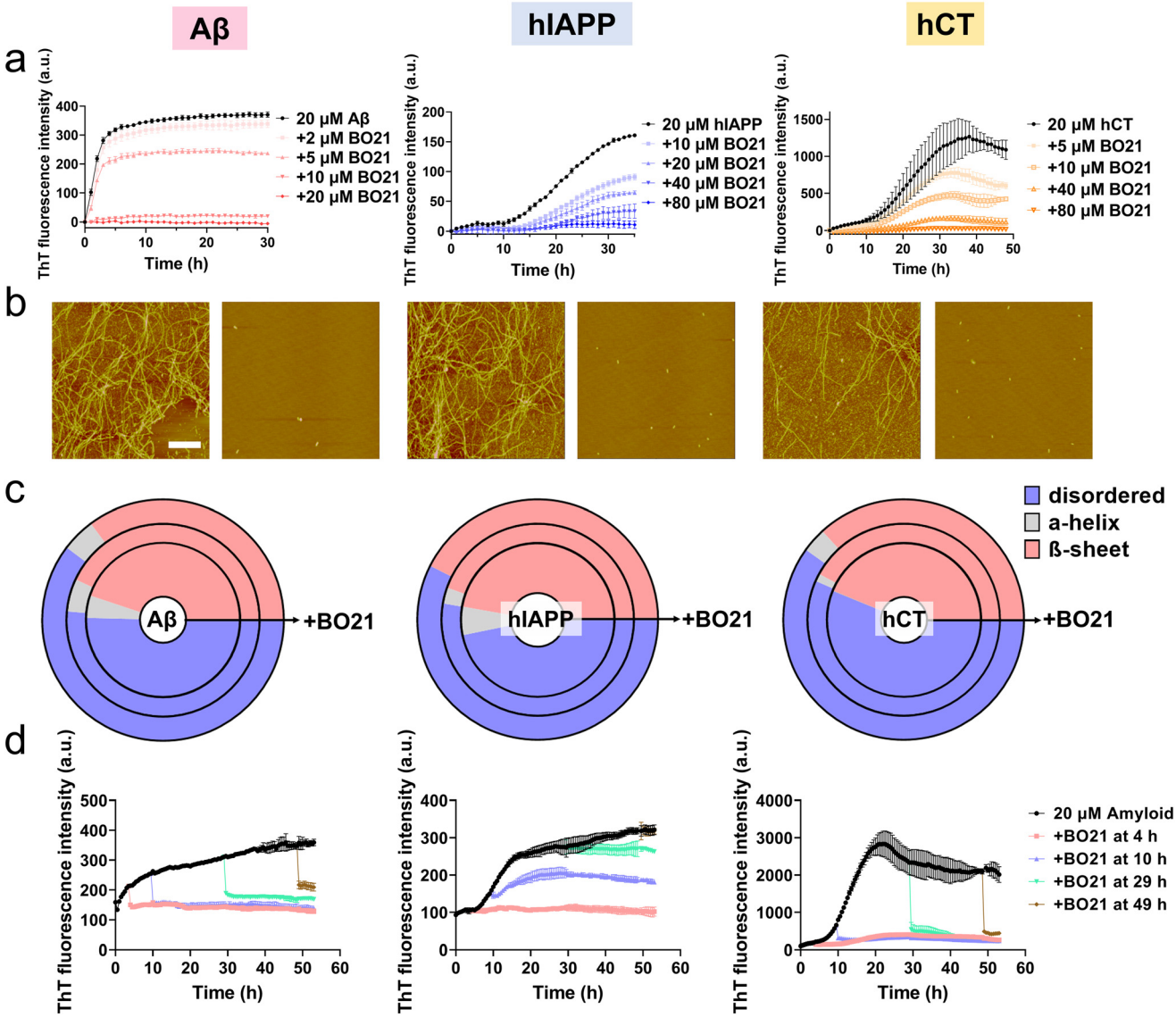

Fig. 5 General inhibition of amyloid fibrillization by BO21. (a) Amyloid aggregation of 20 μM Aβ (1st column), hIAPP (2nd column), and hCT (3rd column) in the absence and presence of 2–80 μM BO21, as monitored by the ThT fluorescence kinetic assay over time. Samples were prepared in ThT (10 μM)–Tris buffer solution (10 mM, pH = 7.4) in a 96-well plate at 37 °C and recorded at every 1 hour interval. (b) Representative AFM images of 20 μM Aβ, hIAPP, and hCT aggregation after 24–48 h incubation with and without 20–80 μM BO21, showing the effect of BO21 on the morphology and size of the aggregates. Scale bars are 1 μm. Samples were prepared in PBS buffer (10 mM, pH = 7.4) at 37 °C. (c) Secondary structure distributions of Aβ, hIAPP, or hCT (20 μM) in the presence of varying concentrations of BO21, ranging from 0 μM (inner cycle) to 5–40 μM (middle cycle) and 20–80 μM (outer cycle), as determined by circular dichroism (CD) spectral analysis using the BESTSEL program. Samples were prepared in PBS buffer (10 mM, pH = 7.4) at 37 °C. (d) Time-dependent ThT fluorescence profile for pure amyloid proteins (black) and the addition of 20–80 μM BO21 to 20 μM Aβ, hIAPP, and hCT seeds pre-incubated for 4 h (red), 10 h (blue), 29 h (green), and 49 h (brown). The time points at which BO21 was added to different amyloid seed solutions are indicated by arrows in the ThT profiles. Samples were prepared in ThT (10 μM) –Tris buffer solution (10 mM, pH = 7.4) in a 96-well plate at 37 °C and recorded at every 1 hour interval.

amyloid binding specificity, thus enabling the quantitative and accurate detection of amyloids (Fig. S4†).

The detection limit of BO21 and ThT was determined by using a fixed concentration of mature amyloid fibrils (20 μM) with varying dye concentrations (0.1 to 1 μM) to fit the fluorescence spectra by the $3\delta/k$ method and the results are summarized in Table S3.† The detection limit of BO21 was found to be exceptionally low, with values of 0.1479 μM, 0.1952 μM, and 0.2687 μM for Aβ, hIAPP, and hCT fibrils, respectively, which were obtained through fitting the fluorescence spectra using the $3\delta/k$ method.[54] These values were accompanied by higher R^2 values of 0.9852, 0.9745, and 0.9528 for Aβ, hIAPP, and hCT fibrils, respectively, highlighting the superior sensitivity and accuracy of BO21 for detecting amyloid fibrils. In comparison, ThT had a detection limit and R^2 value of 0.5333 μM and 0.8365 for Aβ fibrils, 0.4009 μM and 0.9005 for hIAPP fibrils, and an N/A value indicating non-linearity and 0.1616 for hCT fibrils,

respectively (Fig. S5 and S6†). These results demonstrate that BO21 has a significantly lower detection limit and higher linearity than ThT for all types of amyloid fibrils tested.

Next, we conducted a side-by-side comparison of the steady state fluorescence response of BO21 and ThT. As a control, we evaluated the potential interference of 1 μM BO21 in the fibrillation kinetics by co-incubating BO21 with freshly prepared amyloid peptides. The results in Fig. S7† showed no discernable difference in the fibrillation processes with and without BO21, confirming the exclusive function of 1 μM BO21 as an amyloid probe. To ensure that the initial background is minimized and the signal amplification is accurate for detecting amyloid aggregates, we normalized the fluorescence intensity by dividing the fluorescence emission intensity of the BO21/ThT–amyloid systems at different aggregation time points with the fluorescence emission intensity of the BO21/ThT–amyloid systems at t = 0 h. Fig. 4b shows the normalized time-dependent fluorescence response of 1 μM BO21 (dark yellow curve) and ThT (green curve) in the presence of wild-type amyloid peptides (20 μM) undergoing the fibrillization process. The fluorescence curves of the three BO21–amyloid systems showed a similar pattern to the ThT fluorescence curves, with typical nucleation–polymerization kinetics of amyloid fibrillization. This suggests that BO21 is generally sensitive to amyloid fibril formation and has the capacity to function as an amyloid aggregation probe. Compared to ThT, BO21 exhibited better performance in terms of emission intensity and sensitivity towards the earlier amyloid species. This is evidenced by several parameters: (i) comparable or shorter lag phase (t = 11 h *vs.* t = 11 h for Aβ, t = 5 h *vs.* t = 5 h for hIAPP, t = 5 h *vs.* t = 10 h for hCT), (ii) less time to reach half of I_{max} ($t_{1/2}$ = 12.5 h *vs.* $t_{1/2}$ = 13.9 h for Aβ, $t_{1/2}$ = 7.7 h *vs.* $t_{1/2}$ = 9.0 h for hIAPP, $t_{1/2}$ = 13.6 h *vs.* $t_{1/2}$ = 18.5 h for hCT), and (iii) faster aggregation kinetics at $t_{1/2}$ (k = 16.9 t^{-1} *vs.* k = 9.3 t^{-1} for Aβ, k = 43.4 t^{-1} *vs.* k = 18.8 t^{-1} for hIAPP, k = 40.2 t^{-1} *vs.* k = 18.9 t^{-1} for hCT) (Fig. 4c). Consistent with the findings presented in Fig. 3, the earlier and stronger fluorescence enhancement observed for BO21 suggests that it can detect the formation of an intermediate species (*i.e.*, the most toxic form of amyloid oligomers) that is distinct from the monomeric and fibrillar forms of amyloid. On the other hand, BO21 exhibits a stronger fluorescence response than ThT towards amyloid fibrils. Specifically, the fluorescence intensity induced by BO21–amyloid binding was higher by 231% for Aβ, 219% for hIAPP, and 366% for hCT, respectively, as compared to the ThT–amyloid binding systems. Through side-by-side comparisons of ThT and BO21 fluorescence responses to amyloid kinetics, we confirmed that BO21 is a more promising and potential fluorescent probe candidate for monitoring fibrillation and distinguishing between amyloid species, from their monomers to oligomers and fibrils.

Given that both BO21 and ThT contain multiple aromatic rings,[40] we examined their binding mechanisms to determine if BO21 competes for the same binding sites as ThT. This allowed us to determine the competitive binding affinity between the ThT–amyloid and BO21–amyloid systems. To this end, we conducted a series of competitive binding tests. Initially, amyloid fibrils were monitored using either ThT alone at λ_{ex} = 450 nm (light green) or BO21 alone at λ_{ex} = 470 nm (light yellow). Subsequently, the emission signal from the single fluorophore was measured after adding another fluorophore. For example, BO21 was added into ThT-binding amyloid solution and tested at λ_{ex} = 450 nm (dark green), or ThT was added into BO21-binding amyloid solution and tested at λ_{ex} = 470 nm (dark yellow). Since the emission of ThT is not within the range of BO21 absorption, there is no energy transfer between BO21 and ThT. Therefore, any reduction in fluorescence after the addition of the second fluorophore would only indicate the occurrence and efficiency of binding replacement. Fig. 4d shows that the addition of ThT or BO21 as a second fluorophore induced a reduction in the fluorescence spectrum for detecting amyloid fibrils to different extents. Specifically, the addition of BO21 caused a significant reduction in the fluorescence emission of ThT, indicating that BO21 and ThT compete for the same binding sites on amyloid fibrils. However, due to its higher binding affinity to amyloid fibrils, BO21 was able to displace the bound ThT molecules and occupy the binding sites, leading to the fluorescence reduction. Evidently, under 450 nm excitation, BO21 was able to effectively compete with ThT for binding sites, leading to a reduction of the fluorescence peak at 485 nm by 18.6%, 41.5%, and 34.5% for Aβ, hIAPP, and hCT fibril systems, respectively. In contrast, when ThT was added to BO21-bound amyloid fibrils, the binding interaction between amyloid fibrils and BO21 was affected to a lesser extent under 470 nm excitation. The fluorescence spectra showed peak changes of only −3.10%, −18.6%, and −16.9% at 465 nm for Aβ, hIAPP, and hCT fibril systems, respectively. These results suggest that ThT has a lower binding affinity to amyloid fibrils compared to BO21, thus ThT is energetically unfavorable to displace the bound BO21 molecules.

2.3. General inhibition of amyloid fibrillization by BO21

Hypothetically, the amyloid detection property of BO21 is attributed to its ability to strongly interact with amyloid species, which competitively immobilizes the torsional movements of BO21, leading to the emission of strong fluorescence. Moreover, these strong BO21–amyloid interactions may potentially reduce amyloid–amyloid interactions, thereby inhibiting amyloid aggregation and even breaking down preformed amyloid aggregates. To test this hypothesis, we examined the potential inhibition ability of BO21 (2–80 μM) in the presence of freshly prepared Aβ, hIAPP, or hCT (20 μM) with different amyloid : BO21 molar ratios ranging from 1 : 0.1 to 1 : 4 at 37 °C for 30–48 h. As shown in Fig. S8,† incubation of pure BO21 at concentrations ranging from 0.1–80 μM at 37 °C for 48 hours did not produce any detectable fluorescence signal, which rules out the possibility of (i) any fluorescence emission from BO21

itself upon excitation at 450 nm and (ii) any abnormal interactions between BO21 and ThT that could affect the accuracy of the subsequent inhibition tests. As additional controls, Aβ, hIAPP, or hCT alone displayed characteristic sigmoidal nucleation–polymerization curves. Specifically, each curve started with a short lag phase of 0–10 hours, followed by a rapid growth phase of 3–28 hours, and finally reached a saturated phase with the highest ThT intensity of 371, 161, and 1089 a.u., respectively (as indicated by the black lines in Fig. 5a). For comparison, the presence of BO21 resulted in concentration-dependent inhibition of the aggregation kinetics for all three amyloid peptides, as evidenced by (i) an increase in the lag time from 0 h to 36/48 h (*i.e.*, complete inhibition), (ii) a reduction in the aggregation rate during the growth phase, and (iii) a decrease in the final ThT intensity during the equilibrium phase. As a proof-of-concept example, we found that 20 μM BO21 was able to completely suppress equimolar Aβ aggregation. Further decreasing the Aβ : BO21 ratio from 1 : 0.5 to 1 : 0.1 resulted in a reduction of Aβ fibrilization by 8.62%, 36.1%, and 94.8%, indicating general inhibition of Aβ aggregation by binding with Aβ species. As compared to Aβ, a higher concentration of BO21 was required to achieve a comparable level of inhibition for hIAPP and hCT. At molar ratios of BO21 : amyloid = 0.5 : 1 to 4 : 1 and 0.25 : 1 to 4 : 1, BO21 (5–80 μM) significantly inhibited 20 μM amyloid fibril formation of hIAPP by 43.6 to 93.3% and hCT by 44.7 to 98.4%, respectively.

To validate the ThT results, we also recorded AFM images at different time points during the kinetic experiments. The AFM images of the pure amyloid samples (20 μM) showed a large quantity of fibrils being formed after 24 hours of incubation, with an average height/length of 20/2480 nm for Aβ, 16/2588 nm for hIAPP, and 23/2654 nm for hCT. In comparison, co-incubation of 20 μM amyloid peptides with 20 μM (for Aβ) or 80 μM (for hIAPP and hCT) BO21 almost completely suppressed amyloid fibril formation. This was evidenced by the absence of large mature fibers, and instead the presence of many discrete spherical aggregates. Analysis of these aggregates in the AFM images revealed a significant reduction in the average height/length of 13/135 nm for Aβ–BO21, 10/140 nm for hIAPP–BO21, and 12/132 nm for hCT–BO21 systems, respectively (Fig. 5b).

To gain further insight into the inhibition mechanism, we utilized circular dichroism (CD) spectroscopy to monitor changes in the secondary structure of amyloid peptides (20 μM) during fibril formation in the presence and absence of BO21 (5–80 μM) (Fig. 5c and S9–S11†). As a control, all three types of amyloid peptides showed a typical secondary structural transition from a random coil (indicated by the negative peak at 198 nm) to a β-sheet rich structure (indicated by the negative peak at ~215 nm and positive peak at ~195 nm) during self-aggregation. Specifically, at 24–48 h, pure Aβ, hIAPP, and hCT (20 μM) exhibited 50.4%, 46.8%, and 43.7% random coil, 4.7%, 6.0%, and 0.1% α-helix, and 44.9%, 47.2%, and 56.1% β-structure, respectively. In contrast, the co-incubation of BO21 with amyloid peptides resulted in a significant delay in the structural transition of amyloid aggregates from random coil structures to β-sheet structures in a dose-dependent manner, as indicated by the weakened peak at ~215 nm and ~195 nm (Fig. S9–S11†). Specifically, for Aβ aggregates, 5–20 μM BO21 reduced the β-structure content to 35.2–43.1% (Fig. S9†); for hIAPP aggregates, 40–80 μM BO21 reduced the β-structure content to 42.6–44.6% (Fig. S10†); and for hCT aggregates, 40–80 μM BO21 reduced the β-structure content to 36.8–42.1% (Fig. S11†). The CD spectra analysis revealed that the dose-dependent effect of BO21 on reducing the β-structure content in amyloid aggregates varied across different amyloid peptides. Additionally, the results suggested that BO21 inhibits amyloid fibrillization by hindering the conformational changes of amyloid from random coil to β-sheet structures.

While BO21 exhibited strong inhibition of amyloid aggregation from monomers to fibrils, it is also important to examine whether it can inhibit amyloid aggregation from preformed amyloid seeds. To this end, we performed seeding experiments by adding 20 μM (for Aβ)/80 μM (for hIAPP and hCT) BO21 to amyloid seeds (20 μM) that were pre-incubated for 4 h, 10 h, 29 h, and 49 h, covering the lag, growth, and equilibrium phases of Aβ, hIAPP, and hCT aggregation. The inhibitory efficiency was assessed by monitoring changes in the aggregation kinetics (*i.e.*, ThT signals) before and after the addition of BO21 to the amyloid seed solutions. As shown in Fig. 5d, upon adding BO21 to preformed amyloid seeds incubated for different durations, there was a sudden drop in ThT signals indicating a strong inhibitory effect on amyloid aggregation. This observation was evident in all cases and was observed at specific points upon adding BO21. To quantify the inhibitory effect of BO21 on preformed amyloid seeds, we compared the ThT signals before and after adding BO21 to 4 h-, 10 h-, and 29 h-seeded amyloid solutions. The results showed that BO21 significantly reduced the final fibrillization of Aβ/hIAPP/hCT by 102.3%/96.1%/91.7% (red line), 98.0%/61.5%/93.0% (blue line), and 84.5%/25.7%/93.7% (green line), respectively. Notably, BO21 exhibited the ability to act as a "β-sheet breaker" by disassembling preformed Aβ and hCT fibrils, but not hIAPP fibrils that were obtained after 48 hours of incubation. Specifically, at molar ratios of BO21 : amyloid = 1 : 1 and 4 : 1, BO21 reduced the amount of Aβ and hCT fibrils (20 μM) by 66.5% and 82.4%, respectively (brown line). Such a disassembly property of BO21 could potentially serve as an important therapeutic strategy for the treatment of amyloid diseases by removing or remodeling existing amyloid fibrils. On the other hand, given the different residue compositions and sequences of the three amyloid peptides, BO21 showed varying degrees of inhibitory efficiency on different amyloid peptides.

2.4. Alleviation of amyloid-induced cell toxicity by BO21

The aforementioned results demonstrated the dual capacity of BO21 as an amyloid probe for the detection of amyloid aggregates and as an inhibitor of amyloid fibrillization. In order to translate these findings into more clinically relevant applications, it is crucial to evaluate (i) the intrinsic toxicity of BO21 and (ii) its potential neuroprotective effects against amyloid-induced cytotoxicity. To assess the potential neuroprotective effects of BO21 on amyloid-induced cytotoxicity by MTT and LDH assays, we used different cell lines and amyloid proteins for *in vitro* cell toxicity tests. Specifically, we used the human neuroblastoma SH-SY5Y cell line for Aβ- and hCT-related systems, and the rat pancreatic insulinoma RIN-m5F cell line for hIAPP-related systems. Fig. S12† shows that pure BO21 displayed a dose-dependent general cytotoxicity to both cell lines as a control. At low concentrations (0.1–20 μM), BO21 was non- or less toxic to SH-SY5Y/RIN-m5F cells with 90.0–97.1%/87.8–99.3% cell viability and 0.37–7.57%/−0.30–5.48% cytotoxicity, while at high concentrations (40–80 μM), BO21 was highly toxic to SH-SY5Y/RIN-m5F cells with 66.9–88.5%/52.0–93.0% cell viability and 23.1–28.6%/12.0–19.1% cytotoxicity. Additionally, pure Aβ, hIAPP, and hCT (20 μM) caused 48.2%, 45.6%, and 55.0% cell viability and 27.3%, 15.8%, and 22.4% cell apoptosis, respectively, upon 24 h incubation with cells, indicating the high toxicity of amyloid aggregates to the cells (Fig. 6).

To investigate the potential neuroprotective effects of BO21, co-incubation of BO21 with amyloid-treated cells showed that all three BO21–amyloid systems led to an increase in cell viability and a decrease in cytotoxicity to some extent, as compared to their corresponding amyloid systems alone. Thanks to the high inhibition efficiency of BO21 on Aβ aggregation, all tested concentrations of BO21 (*i.e.*, 1–20 μM) were found to be non-toxic to SH-SY5Y cells. Specifically, as BO21 concentrations increased from 1 to 20 μM, BO21 enhanced cell viability from 56.1% to 68.7% and reduced cell toxicity from 20.8% to 1.87% (Fig. 6a), exhibiting a concentration-dependent cell protection manner. In the case of BO21–hIAPP and BO21–hCT systems, the impact of the BO21 concentration on cell viability and cytotoxicity was more complex. Although increasing the BO21 concentration can provide better protection against amyloid aggregation-

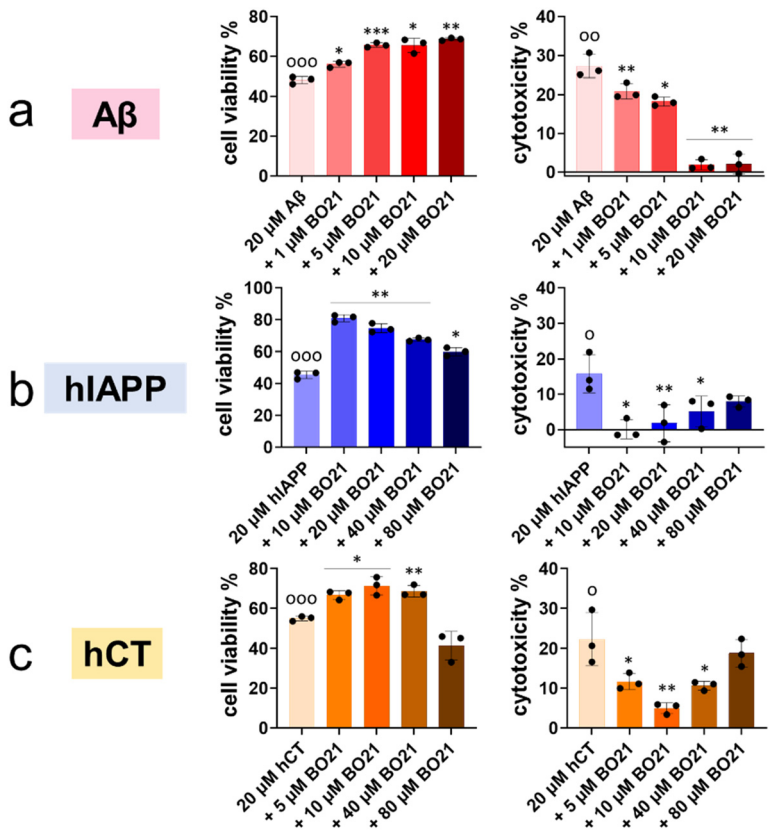

Fig. 6 Rescue of cells from amyloid-induced cytotoxicity by BO21. Dose-dependent cell protection effect of BO21 on amyloid-induced cytotoxicity in (a) Aβ-treated SH-SY5Y cells, (b) hIAPP-treated RIN-m5F cells, and (c) hCT-treated SH-SY5Y cells, as measured by the MTT assay (1st column) and LDH assay (2nd column). Cells were co-treated with amyloid (20 μM) and BO21 (1–80 μM) for 24 h. Statistical analysis was conducted to compare cells treated with amyloid proteins alone to the control group (*, $p < 0.05$; **, $p < 0.01$; ***, $p < 0.001$), as well as to compare cells treated with both BO21 and amyloid proteins to cells treated with amyloid proteins alone (*, $p < 0.05$; **, $p < 0.01$; ***, $p < 0.001$). Data points are depicted as mean values of repeated measurements (n = 3) ± standard errors of the mean. SH-SY5Y/RIN-m5F cells were cultured in 25 cm^2 T-flasks in sterile-filtered ATCCformulated EMEM and F12/RPMI1640 medium containing 10% fetal bovine serum and 1% penicillin/streptomycin.

induced cytotoxicity, it also causes more cell death due to its intrinsic toxicity. Evidently, 10 μM BO21 improved cell viability by 35.4% and decreased cell toxicity by 15.8% in the presence of hIAPP and RIN-m5F cells, but further increasing the concentration of BO21 to 20–80 μM led to a gradual decrease in cell viability to 60.0–74.7% and an increase in cytotoxicity to 1.80–7.99% (Fig. 6b). Similar to the hIAPP–RIN-m5F cell system, as the BO21 concentration increased from 5 to 10 μM, BO21 can protect SH-SY5Y cells from hCT-induced toxicity by improving cell viability by 11.8–16.4% and reducing cell cytotoxicity by 10.7–17.4% (Fig. 6c). However, the cell protection effect of BO21 was weakened when used at concentrations of 40–80 μM, as evidenced by the lower cell viability (41.5–68.7%) and higher cytotoxicity (10.7–18.8%).

3. Conclusions

In this work, we have demonstrated for the first time that BO21 functions as a versatile "dual-function, multi-target" amyloid probe and inhibitor across a range of amyloid peptides, including Aβ (associated with AD), hIAPP (associated with T2D), and hCT (associated with MTC). As an amyloid fluorescence probe, side-by-side comparisons of ThT and BO21 fluorescence responses to different amyloid aggregates confirmed that BO21 is a more promising and potential fluorescent probe candidate for monitoring fibrillation and distinguishing between amyloid species, from their monomers to oligomers and fibrils. BO21 exhibited better performance than ThT in terms of emission intensity and sensitivity towards earlier amyloid species and faster aggregation kinetics. Furthermore, in the presence of amyloid fibrils, BO21 demonstrated a significantly stronger fluorescence response compared to ThT, with fluorescence enhancements ranging from 18–39 fold for Aβ, hIAPP, and hCT fibrils. Overall, the earlier fluorescence enhancement of BO21 suggests that it can detect the formation of intermediates, which are the most toxic species of amyloid oligomers.

Meanwhile, we have demonstrated that BO21 acts as an effective amyloid inhibitor, as evidenced by collective aggregation data from ThT, CD, and AFM experiments. Specifically, BO21 was able to bind with amyloid monomers and oligomers to completely inhibit amyloid aggregation and delay the secondary structure changes to the β-structure by 35.2–44.6%. Additionally, BO21 was able to break down mature amyloid fibrils into small aggregates. Importantly, MTT and LDH cell assays showed that BO21 was able to rescue cells from amyloid-induced cytotoxicity by significantly increasing cell viability by ~7.89–35.4% and reducing cytotoxicity by ~3.53–25.4%, revealing the potential therapeutic value of BO21. These findings suggest that BO21 has significant promise as a potential therapeutic agent for the potential detection and treatment of amyloid-related diseases. In addition, the use of BO21 as a molecular rotor for amyloid detection does have some limitations that should be considered. Firstly, BO21 emits fluorescence in the short/visible wavelength range, which may limit its applicability in certain experimental setups or instrumentation. Secondly, the fluorescence of BO21 can be influenced by environmental factors such as salt concentration, pH, and solvent polarity, which may require careful optimization for different experimental conditions. Lastly, like other molecular rotors, BO21 may exhibit aggregation-induced quenching effects, which could affect its performance in samples with high amyloid concentrations. These limitations should be taken into account when using BO21 as a fluorescent probe for amyloid detection.

4. Experimental procedures

Reagents

Amyloid beta ($A\beta_{1-42}$, ≥95%), human islet amyloid polypeptide ($hIAPP_{1-37}$, purity ≥ 95.0%), and human calcitonin (hCT_{1-32}, purity ≥ 95.0%) were purchased from CPC Scientific (CA, USA). Basic orange 21 (BO21), 1,1,1,3,3,3-hexafluoro-2-propanol (HFIP,99.9%), 10 mM phosphate-buffered saline (PBS, pH = 7.4), dimethyl sulfoxide (DMSO, 99.9%), and thioflavin T (ThT, 98%) were obtained from Sigma-Aldrich (MO, USA). All other chemicals used in this work were of the highest grade.

Peptide purification and preparation

All the peptides were stored at −20 °C immediately once received. To obtain monomeric amyloid peptides, all lyophilized peptides were dissolved in HFIP and incubated at ambient temperature for 2 h, followed by 30 min sonication in an ice bath and 30 min centrifugation at 14 000 rpm and 4 °C, and stored at −80 °C before use. Unless otherwise stated, all peptides were freeze-dried for 1 h and pre-solubilized in DMSO (5% v/v), and then further dissolved in different buffers (Tris buffer/PBS buffer) to reach the desired concentration. The prepared peptide solution must be proceeded on ice and used within 1 h.

Fluorescence light-up detection of amyloid species using BO21 and ThT probes

In the study of using BO21 and ThT as amyloid probes, 40 μM amyloid peptides were incubated to obtain the monomers, oligomers, and fibrils, followed by dilution to 0.625–20 μM. To induce the fluorescence light-up detection, 1 μL luminogen (*i.e.*, BO21 or ThT) was added to 200 μL amyloid solutions and the fluorescence wavelengths were then recorded between 500 and 700 nm/450 and 650 nm with an excitation wavelength of 470 nm (BO21)/450 nm (ThT) by using the kinetic top-read mode of a SpectraMax M3 microplate reader (Molecular Devices, CA, USA).

In order to intuitively observe the "turn on" fluorescence, 40 μM amyloid species of monomers, oligomers, and fibrils stained by 1 μM BO21 were selected to take a photo under

365 nm UV light and further be imaged by fluorescence microscopy under a GFP filter.

The signal/noise ratio (S/N ratio) was calculated by using the fluorescence intensity with (as signal intensity) and without (as noise intensity) amyloid samples at 540 and 480 nm for BO21 and ThT, respectively.

The apparent binding constant K_D of the interaction between BO21 and amyloid species was quantified by titrating BO21 (1 μM) with an increasing amount of amyloid peptides (0–40 μM). Data were analyzed using the 1 : 1 binding model ($\frac{1}{F_t - F_0} = \frac{1}{F_{max} - F_0} + \frac{1}{(F_{max} - F_0)K_D[X]}$, where F_t is the fluorescence intensity during titration, F_0 is the fluorescence intensity before titration, F_{max} is the maximum fluorescence intensity, $[X]$ is the ligand concentration, and K_D is the equilibrium binding constant) and are means (± SD) of three binding curves. Each experiment was repeated at least three times, and each sample was tested in triplicate.

Competition test between BO21 and ThT probes

20 μM amyloid peptides were incubated in PBS buffer for 2 days to ensure the formation of amyloid fibrils. For each well, 1 μL BO21 or ThT was added into the fibrillar amyloid solution to reach the final concentration of 1 μM. The fluorescence wavelengths were then recorded between 500 and 700 nm/450 and 650 nm with an excitation wavelength of 470 nm (BO21)/450 nm (ThT) by using the kinetic top-read mode of a SpectraMax M3 microplate reader (Molecular Devices, CA, USA). To further compare the binding affinity between BO21/ThT and amyloid fibrils, the fluorescence intensity spectra were recorded before and after the addition of another 1 μL ThT or BO21 to the BO21/ThT-binding amyloid solutions. Each experiment was repeated at least three times, and each sample was tested in triplicate.

Determination of detection limits of BO21 and ThT on amyloid fibrils

1 μL luminogen (*i.e.*, BO21 or ThT) was added to 200 μL amyloid solutions (20 μM) to reach the final concentrations of 0.01–1 μM and the fluorescence wavelengths were then recorded between 500 and 700 nm/450 and 650 nm with an excitation wavelength of 470 nm (BO21)/450 nm (ThT) by using the kinetic top-read mode of a SpectraMax M3 microplate reader (Molecular Devices, CA, USA). The detection limits (DLs) of BO21 or ThT for detecting amyloid fibrils were estimated based on the $3\delta/k$ method.

Cross-seeding studies by using the thioflavin T (ThT) fluorescence assay

The amyloidosis kinetics of amyloid peptides were monitored by using the ThT fluorescence assay. To determine the effect of BO21 on monomeric amyloids, samples were prepared on ice by co-incubating freshly prepared Aβ/hIAPP/hCT with 1–80 μM BO21 and 10 μM ThT in Tris buffer. The aggregation kinetics was then initiated at 37 °C and fluorescence intensity data were recorded consistently at 30 min intervals for 48 h. For seeding experiments, a 5 μL BO21–DMSO (20/80 μM) mixture was added into aggregating amyloid solution at 4, 10, 29, and 49 h and aggregation curves were monitored to illustrate the cross-seeding between BO21 and seeded amyloid peptides. The kinetic top-read mode of a SpectraMax M3 microplate reader (Molecular Devices, CA, USA) with excitation at 450 nm and emission in the range of 470 nm to 500 nm was used to monitor the ThT fluorescence.

Atomic force microscopy (AFM)

The morphology changes of amyloid peptides during aggregation were imaged by using a Nanoscope III multimode AFM (Veeco, NY, USA). Samples were prepared by dissolving 20 μM amyloid peptides in DMSO and incubated at 37 °C in the presence or absence of BO21 for 24 h. Then, 10 μL of the samples were deposited on a freshly cleaved mica sheet for 5 min at room temperature, followed by washing three times using Milli-Q water to remove salts and loosely bound peptides and drying with air gas before use. The cantilever resonance frequency was 45–95 kHz. The images (256 pixels × 256 pixels) were captured using a scan size of 5 μm. Representative AFM images were obtained by scanning six different locations on the mica surface.

Circular dichroism spectroscopy (CD)

The secondary structure transition of Aβ aggregation was monitored by far-UV CD spectroscopy with a J-1500 spectropolarimeter (Jasco Inc., Japan) in continuous scanning mode at room temperature. In brief, 20 μM amyloid peptides were incubated at 37 °C in 10 mM phosphate-buffered saline (PBS, pH 7.4) in the presence or absence of 5–80 μM BO21. 150 mL of samples were pipetted into a 1 mm optical path length CD cuvette, and the spectra were scanned between 190 and 250 nm with a step size of 0.5 nm and a scan rate of 50 nm min^{-1}, in all CD measurements after each time interval. To remove the background influence, all spectra were analyzed by subtracting the PBS buffer baseline. The secondary structural contents were determined by using the Beta Structure Selection (BeStSel) algorithm[55] (**https://bestsel.elte.hu/**).

Cell culture

For the Aβ and hCT systems, human SH-SY5Y neuroblastoma cells (ATCC® CRL-2266TM, VA, USA) were used, while for the hIAPP system, rat insulinoma cells RIN-m5F (ATCC® CRL-11605TM, VA, USA) were selected. The SH-SY5Y cells were cultured in sterile-filtered Eagle's minimum essential medium (Sigma-Aldrich, MO, USA) supplemented with 10% fetal bovine serum (FBS) and 1% penicillin/streptomycin. Similarly, the RIN-m5F cells were cultured in sterile-filtered RPMI-1640 medium (Sigma-Aldrich, MO, USA) supplemented with 10% fetal bovine serum (FBS) and 1% penicillin/streptomycin. All the cells were maintained in a humidified incubator with 5% CO_2 at 37 °C until cells reach 80%

confluence. The cells were then harvested by using 0.25 mg mL^{-1} Trypsin/EDTA solution (Sigma Aldrich, MO, USA) and seeded in a 96-well plate (2×10^4 cells per well).

MTT reduction assay

A colorimetric MTT metabolic activity assay was used to determine cell viability. SH-SY5Y/RIN-m5F cells (2×10^4 cells per well) were cultured in a 96-well plate at 37 °C overnight. Then the cell culture medium was replaced by fresh cell culture medium with freshly prepared amyloid peptide/BO21/amyloid peptide–BO21 solutions and cultured for another 24 h at 37 °C under 5% CO_2 in a humidified incubator. After 24 hours, all suspension liquid was removed, replaced by the MTT reagent (Invitrogen, Carlsbad, CA) and incubated for another 4 h at 37 °C. Finally, the resultant formazan crystals were dissolved in dimethyl sulfoxide and the absorbance was measured at 540 nm using a microplate reader. Each sample was repeated at least three times and the cell viability was calculated in comparison with untreated cells.

Lactate dehydrogenase (LDH) cytotoxicity assay

The amyloid-induced cytotoxicity was further evaluated by the LDH assay. The LDH release from the cytoplasm to the medium caused by membrane leakage was measured as a biomarker to quantify the cytotoxicity. The LDH assay was performed using a CyQUANT™ LDH cytotoxicity assay kit (Thermo Fisher Scientific, Waltham, USA). Briefly, 10 μL sterile water and 10× lysis buffer solution were added to each well as a positive and negative control, respectively, and incubated for 45 min with 5% CO_2. Then 50 μL of medium from each well was transferred to a clean 96-well plate, followed by adding 50 μL of reaction mixture, and incubated for another 30 min in the dark. And finally, 50 μL of stop solution was added to each well and the absorbance was measured at 490 nm and 680 nm by using a SpectraMax M3 microplate reader. To determine the LDH activity, the 680 nm absorbance value (background) was subtracted from the 490 nm absorbance before calculation of % cytotoxicity.

The % cytotoxicity was calculated by using the following formula:

$$\%\ \text{cytotoxicity} = \left(\frac{\text{PG-1 treated LDH activity-spontaneous LDH activity}}{\text{maximum LDH activity-spontaneous LDH activity}}\right) \times 100\%$$

Each sample was repeated at least three times and the cell viability was calculated in comparison with untreated cells.

Conflicts of interest

There are no conflicts to declare.

Acknowledgements

We acknowledge financial support from NSF-CBET-2107619. We also trained three high school students – Bowen Zheng from Copley High School, Alice Xu from Hudson High School, and Keven Gong from Western Reserve Academy – by this project.

References

1 M. G. Iadanza, M. P. Jackson, E. W. Hewitt, N. A. Ranson and S. E. Radford, A new era for understanding amyloid structures and disease, *Nat. Rev. Mol. Cell Biol.*, 2018, **19**(12), 755.
2 F. Chiti and C. M. Dobson, Protein misfolding, functional amyloid, and human disease, *Annu. Rev. Biochem.*, 2006, **75**, 333.
3 C. Soto and S. Pritzkow, Protein misfolding, aggregation, and conformational strains in neurodegenerative diseases, *Nat. Neurosci.*, 2018, **21**(10), 1332.
4 J. Gandhi, A. C. Antonelli, A. Afridi, S. Vatsia, G. Joshi, V. Romanov, I. V. Murray and S. A. Khan, Protein misfolding and aggregation in neurodegenerative diseases: a review of pathogeneses, novel detection strategies, and potential therapeutics, *Rev. Neurosci.*, 2019, **30**(4), 339.
5 A. Gámez, P. Yuste-Checa, S. Brasil, Á. Briso-Montiano, L. R. Desviat, M. Ugarte, C. Pérez-Cerdá and B. Pérez, Protein misfolding diseases: prospects of pharmacological treatment, *Clin. Genet.*, 2018, **93**(3), 450.
6 D. Milardi, E. Gazit, S. E. Radford, Y. Xu, R. U. Gallardo, A. Caflisch, G. T. Westermark, P. Westermark, C. L. Rosa and A. Ramamoorthy, Proteostasis of islet amyloid polypeptide: a molecular perspective of risk factors and protective strategies for type II diabetes, *Chem. Rev.*, 2021, **121**(3), 1845.
7 K. Kamgar-Parsi, J. Tolchard, B. Habenstein, A. Loquet, A. Naito and A. Ramamoorthy, Structural biology of calcitonin: from aqueous therapeutic properties to amyloid aggregation, *Isr. J. Chem.*, 2017, **57**(7–8), 634.
8 L. Clare, Awareness in early-stage Alzheimer's disease: a review of methods and evidence, *Br. J. Clin. Psychol.*, 2004, **43**(2), 177.
9 P. H. Nguyen, A. Ramamoorthy, B. R. Sahoo, J. Zheng, P. Faller, J. E. Straub, L. Dominguez, J.-E. Shea, N. V. Dokholyan and A. De Simone, Amyloid oligomers: A joint experimental/computational perspective on Alzheimer's disease, Parkinson's disease, type II diabetes, and amyotrophic lateral sclerosis, *Chem. Rev.*, 2021, **121**(4), 2545.
10 Y. Zhang, B. Ren, D. Zhang, Y. Liu, M. Zhang, C. Zhao and J. Zheng, Design principles and fundamental understanding of biosensors for amyloid-β detection, *J. Mater. Chem. B*, 2020, **8**(29), 6179.
11 A. Aliyan, N. P. Cook and A. A. Martí, Interrogating amyloid aggregates using fluorescent probes, *Chem. Rev.*, 2019, **119**(23), 11819.
12 Y. Tang, D. Zhang, X. Gong and J. Zheng, Dual-Functional, Multi-Targeting GNNQQNY-AIE Conjugates as Amyloid

Probes and Amyloid Modulators via Amyloid Cross-Seeding Principle, *Adv. Funct. Mater.*, 2022, **32**(45), 2208022.
13 M. Ono and H. Saji, Recent advances in molecular imaging probes for β-amyloid plaques, *MedChemComm*, 2015, **6**(3), 391.
14 P. Vassar, C. Culling and H. Taylor, *Am. J. Pathol.*, 1959, 718.
15 A. Srivastava, P. K. Singh, M. Kumbhakar, T. Mukherjee, S. Chattopadyay, H. Pal and S. Nath, Identifying the bond responsible for the fluorescence modulation in an amyloid fibril sensor, *Chem. – Eur. J.*, 2010, **16**(30), 9257.
16 M. A. Leissring, A. Lu, M. M. Condron, D. B. Teplow, R. L. Stein, W. Farris and D. J. Selkoe, Kinetics of amyloid β-protein degradation determined by novel fluorescence-and fluorescence polarization-based assays, *J. Biol. Chem.*, 2003, **278**(39), 37314.
17 T. Branch, P. Girvan, M. Barahona and L. Ying, Introduction of a Fluorescent Probe to Amyloid-β to Reveal Kinetic Insights into Its Interactions with Copper (II), *Angew. Chem.*, 2015, **127**(4), 1243.
18 A. M. Streets, Y. Sourigues, R. R. Kopito, R. Melki and S. R. Quake, Simultaneous measurement of amyloid fibril formation by dynamic light scattering and fluorescence reveals complex aggregation kinetics, *PLoS One*, 2013, **8**(1), e54541.
19 A. Sidhu, J. Vaneyck, C. Blum, I. Segers-Nolten and V. Subramaniam, Polymorph-specific distribution of binding sites determines thioflavin-T fluorescence intensity in α-synuclein fibrils, *Amyloid*, 2018, **25**(3), 189.
20 N. Amdursky, M. H. Rashid, M. M. Stevens and I. Yarovsky, Exploring the binding sites and proton diffusion on insulin amyloid fibril surfaces by naphthol-based photoacid fluorescence and molecular simulations, *Sci. Rep.*, 2017, **7**(1), 1.
21 A. Alghamdi, S. Forbes, D. J. Birch, V. Vyshemirsky and O. J. Rolinski, Detecting beta-amyloid glycation by intrinsic fluorescence-Understanding the link between diabetes and Alzheimer's disease, *Arch. Biochem. Biophys.*, 2021, **704**, 108886.
22 Y. Tang, D. Zhang, Y. Zhang, Y. Liu, Y. Miller, K. Gong and J. Zheng, Cross-seeding between Aβ and SEVI indicates a pathogenic link and gender difference between alzheimer diseases and AIDS, *Commun. Biol.*, 2022, **5**(1), 1.
23 Y. Zhang, Y. Tang, Y. Liu, D. Zhang and J. Zheng, Design and engineering of amyloid aggregation-prone fragments and their antimicrobial conjugates with multi-target functionality, *Adv. Funct. Mater.*, 2021, **31**(32), 2102978.
24 M. T. Elghetany and A. Saleem, Methods for staining amyloid in tissues: a review, *Stain Technol.*, 1988, **63**(4), 201.
25 Y. Tang, Y. Liu, Y. Zhang, D. Zhang, X. Gong and J. Zheng, Repurposing a Cardiovascular Disease Drug of Cloridarol as hIAPP Inhibitor, *ACS Chem. Neurosci.*, 2021, **12**(8), 1419.
26 Y. Tang, D. Zhang, Y. Zhang, Y. Liu, X. Gong, Y. Chang, B. Ren and J. Zheng, Introduction and Fundamentals of Human Islet Amyloid Polypeptide Inhibitors, *ACS Appl. Bio Mater.*, 2020, **3**(12), 8286.
27 H. Levine III, Stopped-flow kinetics reveal multiple phases of thioflavin T binding to Alzheimer β (1-40) amyloid fibrils, *Arch. Biochem. Biophys.*, 1997, **342**(2), 306.
28 A. A. Maskevich, V. I. Stsiapura, V. A. Kuzmitsky, I. M. Kuznetsova, O. I. Povarova, V. N. Uversky and K. K. Turoverov, Spectral properties of thioflavin T in solvents with different dielectric properties and in a fibril-incorporated form, *J. Proteome Res.*, 2007, **6**(4), 1392.
29 M. D'Amico, M. G. Di Carlo, M. Groenning, V. Militello, V. Vetri and M. Leone, Thioflavin T promotes Aβ (1–40) amyloid fibrils formation, *J. Phys. Chem. Lett.*, 2012, **3**(12), 1596.
30 I. M. Kuznetsova, A. I. Sulatskaya, V. N. Uversky and K. K. Turoverov, Analyzing thioflavin T binding to amyloid fibrils by an equilibrium microdialysis-based technique, *PLoS One*, 2012, **7**(2), e30724.
31 Z. Eizig Bar-On, M. A. Iron, H. L. Kasdan, D. Amir, E. Afrimzon, N. Zurgil, S. Moshkov and M. Deutsch, The cationic dye basic orange 21 (BO21) as a potential fluorescent sensor, *Photochem. Photobiol. Sci.*, 2018, **17**, 1417.
32 Z. Geng, Y. Zhang, Y. Gou, J. Zhou, L. Guo and Q. Wu, Identification of a New Adulterated Dye and Study on Detection Method for 9 Orange-yellow Dyes in Typhae Pollen, *Zhongguo Yaofang*, 2017, 1225.
33 Z. R. Grabowski, K. Rotkiewicz and W. Rettig, Structural changes accompanying intramolecular electron transfer: focus on twisted intramolecular charge-transfer states and structures, *Chem. Rev.*, 2003, **103**(10), 3899.
34 S. P. Pandey and P. K. Singh, Basic Orange 21: a molecular rotor probe for fluorescence turn-on sensing of amyloid fibrils, *J. Mol. Liq.*, 2020, **303**, 112618.
35 G. Singh, V. R. Singh, S. P. Pandey and P. K. Singh, Sulfated-β-cyclodextrin templated aggregation of a metachromatic dye, Basic Orange 21: A photophysical investigation, *Supramol. Chem.*, 2021, **33**(8), 460.
36 G. Singh, S. P. Pandey and P. K. Singh, Anionic Polyelectrolyte-Induced Aggregation of Basic Orange 21: A Clue toward Metachromasia, *J. Phys. Chem. B*, 2021, **125**(25), 7033.
37 Z. Eizig, D. T. Major, H. L. Kasdan, E. Afrimzon, N. Zurgil, M. Sobolev and M. Deutsch, Analysis of the spectroscopic aspects of cationic dye basic orange 21, *J. Phys. Chem. A*, 2015, **119**(38), 9794.
38 L. Kass, Individual leukocyte determination by means of differential metachromatic dye sorption, US4581223, 1986.
39 Z. Eizig, D. Major, H. Kasdan, E. Afrimzon, N. Zurgil and M. Deutsch, *Spectroscopic Characteristics of the Cationic Dye Basic Orange 21 in Leukocytes*, 2014.
40 M. Groenning, Binding mode of Thioflavin T and other molecular probes in the context of amyloid fibrils—current status, *J. Chem. Biol.*, 2010, **3**, 1.
41 A. Lorenzo and B. A. Yankner, Beta-amyloid neurotoxicity requires fibril formation and is inhibited by congo red, *Proc. Natl. Acad. Sci. U. S. A.*, 1994, **91**(25), 12243.
42 A. K. Mora, P. K. Singh, B. S. Patro and S. Nath, PicoGreen: a better amyloid probe than Thioflavin-T, *Chem. Rev.*, 2016, **52**(82), 12163.

43 N. H. Mudliar and P. K. Singh, A molecular rotor-based turn-on sensor probe for amyloid fibrils in the extreme near-infrared region, *Chem. Commun.*, 2019, **55**(27), 3907.
44 M. Sulatsky, A. Sulatskaya, O. Povarova, I. A. Antifeeva, I. Kuznetsova and K. Turoverov, Effect of the fluorescent probes ThT and ANS on the mature amyloid fibrils, *Prion*, 2020, **14**(1), 67.
45 S. P. Pandey, T. Dutta, B. Chakraborty, A. L. Koner and P. K. Singh, Mitochondria-Directing Fluorogenic Probe: An Efficient Amyloid Marker for Imaging Lipid Metabolite-Induced Protein Aggregation in Live Cells and Caenorhabditis elegans, *Anal. Chem.*, 2023, **95**(15), 6341.
46 O. D. Warerkar, N. H. Mudliar and P. K. Singh, A hemicyanine based fluorescence turn-on sensor for amyloid fibril detection in the far-red region, *J. Mol. Liq.*, 2021, **328**, 115322.
47 M. H. Aarabi and S. M. Mirhashemi, To estimate effective antiamyloidogenic property of melatonin and fisetin and their actions to destabilize amyloid fibrils, *Pak. J. Pharm. Sci.*, 2017, **30**(5), 1589.
48 R. Dubey, K. Patil, S. C. Dantu, D. M. Sardesai, P. Bhatia, N. Malik, J. D. Acharya, S. Sarkar, S. Ghosh and R. Chakrabarti, Azadirachtin inhibits amyloid formation, disaggregates pre-formed fibrils and protects pancreatic β-cells from human islet amyloid polypeptide/amylin-induced cytotoxicity, *Biochem. J.*, 2019, **476**(5), 889.
49 B. Ren, Y. Liu, Y. Zhang, Y. Cai, X. Gong, Y. Chang, L. Xu and J. Zheng, Genistein: a dual inhibitor of both amyloid β and human islet amylin peptides, *ACS Chem. Neurosci.*, 2018, **9**(5), 1215.
50 A. N. Khan, F. Nabi and R. H. Khan, Mechanistic and biophysical insight into the inhibitory and disaggregase role of antibiotic moxifloxacin on human lysozyme amyloid formation, *Biophys. Chem.*, 2023, **298**, 107029.
51 Y. Hong, L. Meng, S. Chen, C. W. T. Leung, L.-T. Da, M. Faisal, D.-A. Silva, J. Liu, J. W. Y. Lam and X. Huang, Monitoring and inhibition of insulin fibrillation by a small organic fluorogen with aggregation-induced emission characteristics, *J. Am. Chem. Soc.*, 2012, **134**(3), 1680.
52 L.-M. Yan, M. Tatarek-Nossol, A. Velkova, A. Kazantzis and A. Kapurniotu, Design of a mimic of nonamyloidogenic and bioactive human islet amyloid polypeptide (IAPP) as nanomolar affinity inhibitor of IAPP cytotoxic fibrillogenesis, *Proc. Natl. Acad. Sci. U. S. A.*, 2006, **103**(7), 2046.
53 P. Thordarson, Determining association constants from titration experiments in supramolecular chemistry, *Chem. Soc. Rev.*, 2011, **40**(3), 1305.
54 C. Fan, Z.-Q. Chen, C. Li, Y.-L. Wang, Q. Yu and M.-Q. Zhu, Hydrophilic AIE-Active tetraarylethenes for fluorescence sensing and super-resolution imaging of amyloid fibrils from hen egg white lysozyme, *ACS Appl. Mater. Interfaces*, 2021, **13**(17), 19625.
55 A. Micsonai, F. Wien, L. Kernya, Y.-H. Lee, Y. Goto, M. Réfrégiers and J. Kardos, Accurate secondary structure prediction and fold recognition for circular dichroism spectroscopy, *Proc. Natl. Acad. Sci. U. S. A.*, 2015, **112**(24), E3095.